Received: 25 July 2025 | Revised: 13 November 2025 | Accepted: 31 December 2025 | Published online: 9 February 2026

RESEARCH ARTICLE

Remote Sensing for Sustainable Oceans
2026, Vol. 00(00) 1–8
DOI: 10.47852/bonviewRSSO62026936

BON VIEW PUBLISHING

Observing the Linkage of Atmospheric and Oceanic Front Using Remote Sensing Observations: A Case Study After the Passage of Tropical Cyclone Asani

Bipasha Paul Shukla[1], Suchandra Aich Bhowmick[1,*], Anup Kumar Mandal[1] and Abhisek Chakraborty[1]

[1] *Atmospheric and Oceanic Sciences Group, Indian Space Research Organisation, India*

Abstract: The Marine Atmospheric Boundary Layer (MABL) is a hub of several important and dynamic phenomena, including eddies, gravity waves, atmospheric fronts, rolls, convective cells, etc. In particular, shear-induced and convective eddies drive the energy transfer from the ocean surface to the atmosphere. This energy transfer, in turn, is one of the key factors orchestrating the atmosphere-ocean dynamics. Using the data from the Earth Observation Satellite (EOS-04), a case study is conducted to examine frontal features in the ocean-atmosphere system. SAR and complementary data (Sentinel-3, GHRSST, and ECMWF) reveal the coeval emergence of oceanic and atmospheric fronts, thereby establishing a strong linkage between them. The concurrent presence of cyclone Asani suggests that the traversal of a cyclonic disturbance in the vicinity could account for this phenomenon. Tropical cyclones frequently generate a pronounced cold wake in the upper ocean; however, concurrent observations of both oceanic and atmospheric frontal boundaries in these environments remain uncommon. This study documents a unique instance of simultaneous air-sea frontal structures following a cyclone. These findings indicate coupled feedback mechanisms in which oceanic thermal gradients influence near-surface winds, while atmospheric forcing contributes to frontogenesis. This concurrent observational evidence highlights the significance of cyclone-induced cold-wake fronts as regions of active air-sea interaction, with potential consequences for regional weather prediction, upper-ocean biogeochemistry, and post-cyclone recovery processes.

Keywords: EOS-04, SAR, MABL, atmospheric fronts, cyclone

1. Introduction

Atmospheric fronts delineate boundaries between contrasting air masses and exert a significant influence on meteorological phenomena, particularly in the occurrence of severe precipitation events. Air masses originate in prominent high-pressure areas across the globe and acquire distinct temperature and humidity characteristics through prolonged interaction with the underlying surface. These distinct air masses, characterized by diverse physical properties, often exhibit disparate wind speeds on either side, giving rise to the formation of fronts [1]. Notably, when stationary fronts dissipate into narrower scales, they manifest as shear lines that serve as focal points for various severe weather phenomena [2, 3]. Although their occurrence is more prevalent in mid-latitude regions [4], the impact of fronts in tropical areas should not be underestimated [5]. The understanding of these frontal processes and their impact on weather patterns is crucial for accurate management of precipitation-related hazards. For example, Parfitt et al. [6] showed the response of atmospheric fronts to a change in the sea surface temperature (SST) gradient in the Gulf Stream region.

Cyclones find a special association with fronts [7]. Mid-latitude or extratropical cyclones are distinctly characterized by the fronts that spiral out from their low-pressure center. Ahead of the cyclone center lies the warm front, where advancing warm air rises over the colder air mass, typically resulting in a broad area of light, steady precipitation and gradually increasing cloud cover. Following the warm sector is the faster-moving cold front, which signals the colder air mass pushing under and rapidly lifting the remaining warm air; this interaction creates a much narrower, more intense band of weather, often featuring heavy rain, strong thunderstorms, and a sharp temperature drop. As the cyclone matures, the faster-moving cold front may overtake the warm front, forming an occluded front that marks the end of the storm's intensification phase.

In general, the wind stress and thus the small-scale sea surface roughness change across atmospheric fronts. In the synthetic aperture radar (SAR) images, they can be viewed as structured lines separating areas of differing normalized radar cross-section (NRCS) values. Precisely, SAR images capture the physical response of the ocean surface to the wind field and its variations associated with an atmospheric front. The optical remote sensing of frontal features encounters significant challenges due to extensive cloud cover. By overcoming this limitation, SAR data presents a valuable opportunity for investigating atmospheric fronts. SAR exploits the distinctive modifications that fronts induce on the sea surface, resulting in small-scale roughness changes primarily driven by capillary and ultra-gravity waves. As sea roughness intensifies, the backscattered radar power or NRCS increases, leading to lighter gray tones in SAR imagery (in a grayscale image). Thus, SAR, with its all-weather capability, broad spatial coverage, and superior spatial resolution, is a potent tool for capturing atmospheric fronts. Moreover, SAR data provides valuable insights into the distribution of oceanic rain cells [8] embedded within frontal systems, allowing for a more comprehensive understanding of their dynamics and associated precipitation patterns.

***Corresponding author:** Suchandra Aich Bhowmick, Atmospheric and Oceanic Sciences Group, Indian Space Research Organisation, India. Email: suchandra@sac.isro.gov.in

Nonetheless, it is important to acknowledge that variations in small-scale sea-surface roughness may have origins other than wind stress variations. For instance, fluctuations in surface currents associated with oceanic fronts can introduce variability in small-scale sea-surface roughness through wave-current interaction, consequently affecting NRCS variations. Rainfall and thunderstorms are often observed along frontal boundaries, further complicating the interpretation of SAR data and the identification of fronts. However, the gray levels in SAR images, which relate to the NRCS, may not be solely indicative of rain cells due to raindrop impacts. Dark areas or regions of reduced NRCS values can be caused by various factors, including natural surface films from plankton or fish, low wind conditions near islands or coastal mountains, cold upwelling waters affecting the air-sea interface, divergent flow patterns such as internal waves, etc. [9]. In essence, the dark areas appear in SAR images due to divergence of currents that stretches the sea surface, reducing short-wave roughness and damping of short waves due to surface films.

Consequently, the identification and analysis of atmospheric fronts remain challenging tasks that necessitate a multidisciplinary approach. Integrating ancillary observations and model analyses alongside SAR data can enhance our understanding of the complex processes occurring within the marine atmospheric boundary layer (MABL) [10]. This comprehensive approach enables a more robust examination of the oceanic and thermodynamic factors driving frontogenesis, facilitates differentiation among various frontal categories, and provides insights into the structures embedded within frontal zones, such as oceanic rain cells. The launch of the recent SAR (EOS-04) extends the potential detection and analysis of the MABL structures over the Indian Ocean [11].

In this manuscript, we explore the case of an atypical atmospheric front, which manifests in an oceanic front as well. By utilizing various satellite and modeling observations, we examine how the interactions between the atmosphere and ocean influence this occurrence and attempt to identify connections with a nearby tropical cyclone. The following sections outline the data utilized, the methodology employed, and the results along with the discussion.

2. Dataset

Since the atmospheric fronts are often associated with clouds, detecting one using optical remote sensing data may not be feasible. Thus, in this study, we utilized the EOS-04 SAR that operates in the microwave range for the identification of fronts. For the present study, we have used Level-2 (L2) geo-referenced data (bhoonidhi.nrsc.gov.in) acquired in Medium Resolution SCANSAR (MRS) mode in HH polarization from the C-band SAR onboard EOS-04 launched on February 14, 2022, by Indian Space Research Organisation (ISRO). The pixel spacing for the data in both range and azimuth directions is 18 m. The geolocation accuracy of the products is better than 50 m. The radiometric accuracy is ~ 1 dB.

SAR has all-weather capability and potential to detect fronts in form of patches in the data. However, as discussed, these patches can have many probable reasons apart from being a front. Thus, we require data from other sources too for discriminating these dark patches as a front. We, therefore, have also used the full-resolution Level-1 top-of-atmosphere reflectance data (visible and near infrared) from the Ocean and Land Color Instrument (OLCI) onboard the Sentinel-3 satellite provided by the European Space Agency (ESA). This full-resolution product has a grid resolution of 300 m, and the geometric accuracy is within 100 m.

To analyze the characteristics of the air masses forming the front, we have also used ERA5 [12], which is the latest iteration of the European Centre for Medium-Range Weather Forecasts (ECMWF) reanalysis. With a global reach and a spatial resolution of approximately 31 km, ERA5 provides hourly data from 1950 to the present, with new information available within 5 days of observation. ERA5 includes data on a wide range of atmospheric variables, including wind speed and direction, temperature, humidity, and precipitation. While acknowledging that the product exhibits certain limitations under specific conditions, it is imperative to emphasize that ERA5 remains a valuable resource for research when utilized judiciously.

The corresponding ocean conditions were explored using the SST data. The Group for High-Resolution Sea Surface Temperature (GHRSST) data used here is a merged sea surface temperature (SST) product that includes observations from all the available microwave and infrared sensors. The Level-4 (L4) product is generated using various objective analysis techniques to produce gap-free SST maps over the global oceans. The SST product used in this study is generated by Jet Propulsion Laboratory (JPL) using an optimum interpolation approach on a global 0.011° grid [13]. This is a version 4 multiscale ultrahigh resolution (MUR) product that has inputs from many sources of SST such as NASA Advanced Microwave Scanning Radiometer-EOS (AMSRE), the Moderate Resolution Imaging Spectroradiometer (MODIS) on the NASA Aqua and Terra platforms, the US Navy microwave WindSat radiometer, and in situ SST observations from the NOAA iQuam project. GHRSST SST products are blended from multiple satellites or multiple passes of satellites [14]. The data were obtained for the entire month of May 2022 from this URL: https://podaac-tools.jpl.nasa.gov/drive/files/allData/ghrsst/data/GDS2/L4/GLOB/JPL/MUR/v4.1.

3. Methodology

The EOS-04 SAR data used in this study have the advantage of all-weather capability, making SAR an extremely important remote sensing instrument for studying fronts, which are often associated with clouds and precipitation. EOS-04 has been judiciously calibrated using corner reflectors installed at Ahmedabad and Amrapur in the state of Gujarat, India, as discussed by Sharma et al. [15]. The evaluation of the data in terms of radiometric, geometric, and polarimetric calibration showed satisfactory performance of SAR with an absolute calibration accuracy within 2 dB and a stable backscatter coefficient. In this case, processing of the SAR data including filtering the noise in EOS-04 GeoTIFF MRS data is carried out and is described as follows:

1) The input MRS data contain the digital number (*DN*). The backscatter coefficient (σ_0) is computed from *DN* using the formula provided in the EOS-04 manual:

$$\sigma_0 = \frac{(DN_p^2 - N) \times sini_p}{K_{Cal_{Beta0_{linear}}}},$$

$$K_{cal\_Beta0\_linear} = 10^{\left(\frac{Kcal\_Beta0\_db}{10}\right)}$$

where DN_p is the digital number or the image pixel gray-level count for the pixel p, i_p is the local incidence angle for pixel p and it is given in the *_lia.tif file with the product, $K_{Cal\_Beta0\_linear}$ is the product radiometric calibration constant in linear scale which is obtained from *KCal_Beta0_db* (given in the "BAND_META.txt" file), and N is the image noise bias, obtained from the "BAND_META.txt" file.

2) After computing the σ_0 in the linear scale, we found that it is negative at poor SNR pixels. The poor SNR pixels are those pixels for which $DN_p^2 < N$. The negative σ_0 values at some of the pixels need to be handled by the user depending on the scientific application (EOS-04 Manual). Initially, such poor SNR pixels are identified using the threshold (where $\sigma_0 < 0$ and replaced with NaN values. However, for this case, no such pixels were found.
3) For most of the applications, granular noise in the data needs to be removed. This is performed through speckle filtering (median

filter of kernel size 11 x 11) available in the SciPy Python library. In the final step, $\sigma_0(lin)$, $\sigma_0(dB)$, incidence angle (i_p), and azimuth angle along with latitude and longitude information are stored in a NetCDF file, which can be conveniently used for many applications instead of using the raw data.

Using the processed backscatter of the EOS-04, we observed patches over the Indian Ocean on May 12, 2022, that can be a probable front. To cross-check, images acquired by the OLCI instrument onboard the Sentinel-3 satellite were also examined, revealing the presence of associated cloud patches. To verify and analyze the nature of the air masses in terms of humidity and geopotential height, ERA5 data were used. The three-dimensional (3D) time series of humidity and the time series of geopotential height were constructed for the period from 07:00 UTC on May 11, 2022, to 11:00 UTC on May 12, 2022. These 3D time series are constructed for a given area between 80° E and 90° E and 10° N and 20° N at pressure levels between 1000 hPa and 2000 hPa.

We have also used the GHRSST data to analyze the ocean conditions. As mentioned, GHRSST provides SST observations from various sources. Thus, the absolute errors for the data are not single, fixed values. They are dynamic, varying with product type, sensor, and spatiotemporal factors. The GHRSST community quantifies these errors using metrics known as Single Sensor Error Statistics (SSES), which include bias and standard deviation. Errors in these products are primarily due to sensor bias, instrument noise, and sampling uncertainty. Further, satellite infrared sensors measure the temperature of the top few micrometers of the ocean surface, referred to as the skin temperature, whereas most in situ buoys measure the temperature at a greater depth. The two measurements can differ by approximately 0.17 K, with the skin temperature generally being cooler. This also contributes to the errors in such products. The GHRSST Multi-Product Ensemble (GMPE) is a blended product that combines multiple SST analyses into a single, statistically robust, and unbiased median, making it useful for climate monitoring and inter-comparison. The MUR product is a single high-resolution SST dataset created by blending satellite and in situ observations, suitable for studying fine-scale ocean features. However, validation of a GHRSST L4 product against in situ data often showed good agreement with a small regional cool bias of around 0.1 K. Chin et al. [14] showed that MUR SSTs have a fair match with GMPE globally within 0.36 K.

Apart from analyzing the GHRSST data, we have also computed the SST front [16] using the following expression:

$$SST\ FRONT\ = \sqrt{\left(\frac{\partial sst}{\partial x}\right)^2 + \left(\frac{\partial sst}{\partial y}\right)^2}$$

The ∂x and ∂y represent the variations in the West to East and South to North directions, respectively, over which SST variability is observed.

4. Results and Discussion

In Figure 1, the demarcated boundary of the front can be easily identified in the EOS-04 SAR image acquired on May 12, 2022. This is identified in terms of the higher backscattering coefficient of EOS-04. The red box in Figure 1 shows the area of high backscatter as compared to its surrounding. Further, since fronts are often associated with changes in wind direction and speed, the ECMWF winds have been superimposed over the NRCS. To cross-verify the presence of fronts, cloud patches similar to Figure 1 are also observed in the top-of-atmosphere (TOA) reflectance captured by OLCI (Figure 2) along with cyclone Asani near the East Indian Andhra coast.

Rain or thunderstorms often occur along the frontal zone. Due to quasi-geostrophic theory, it is postulated that due to the differential advection in a horizontal deformation field, a thermodynamically direct

Figure 1
EOS-04 SAR scene (Scene No. 18) acquired on May 12, 2022, at 00:11 GMT, with ECMWF wind vectors superimposed. The red box indicates the frontal region

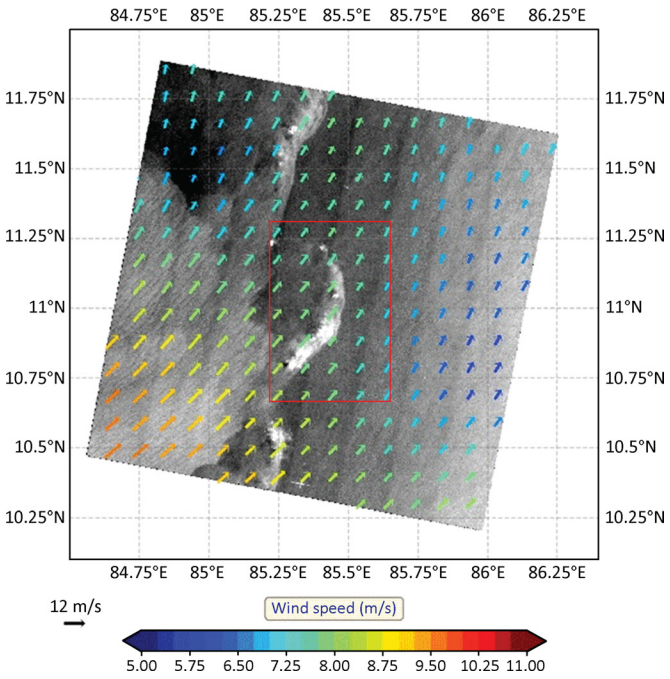

vertical circulation is developed, whenever the horizontal temperature gradient increases, in order to produce a corresponding increase in the vertical wind shear [17].

The temporal three-dimensional humidity plots presented in Figure 3 reveal a discernible frontal boundary in the vicinity of the 500 mb level after 23:00 UTC on May 11, 2023, and this development is attributed to the intrusion of dry air at this atmospheric layer. It can be clearly deduced that this temporal progression aligns seamlessly with the observation of the frontal boundary in EOS-04 SAR data. By tracing the emergence and evolution of the frontal boundary in three dimensions,

Figure 2
Image acquired by ocean and land color imager (OLCI) instrument onboard Sentinel-3 satellite on May 12, 2022, 04:26 UTC. The cyclone Asani is seen in the right panel image near the coastal region of Andhra Pradesh

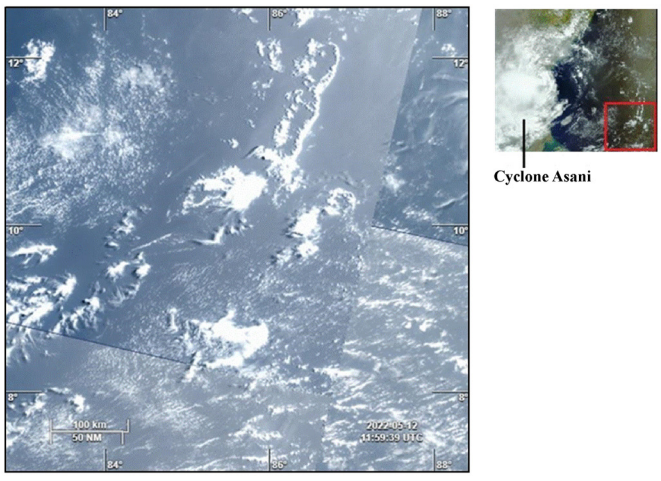

Figure 3
Time series of 3D humidity plots (07:00 UTC, May 11, 2022, to 11:00 UTC, May 12, 2022)

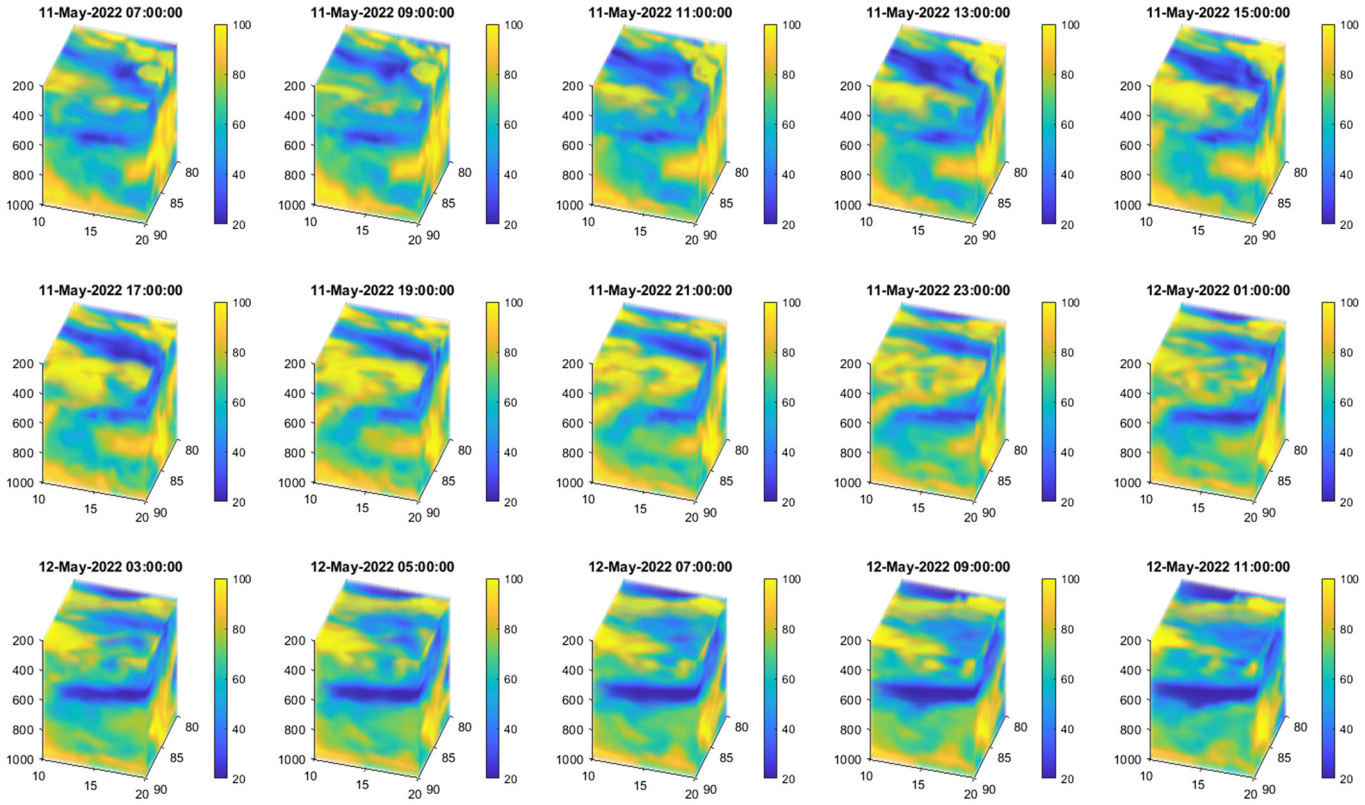

with a particular focus on the 500 mb level, we bring forth the linkage between dry air intrusion and the formation of frontal boundaries. The persistence of dry air plume, as seen through the temporal plots, can also be responsible for evaporation of rain drops, thus explaining the absence of rain. The source of this dry air is hypothesized to be closely linked to the passage of cyclone Asani, as described subsequently. As a cyclone develops and progresses over the ocean, air rises within the eyewall and rain bands, losing moisture and cooling as it ascends. This dry, cold air eventually sinks in the eye and areas between the rain bands. Throughout this process, the air loses moisture, leading to the formation of descending dry air. Earlier studies and modelling experiments [18] have shown dry air descent during tropical cyclone evolution, which can impact its strength. It is known that, after a cyclone passes, it is commonly succeeded by dry air descending, or subsidence, as the atmosphere seeks to regain balance. During the storm, large amounts of warm, humid air ascend quickly into the atmosphere, forming a significant low-pressure system. When the cyclone disperses, an anticyclone—a high-pressure system identified by descending air—typically enters the region to take its place. This may have been the persistent dry air that reinforced the frontal boundary as seen in the figure.

Geopotential height (GH) is another valuable parameter for analyzing atmospheric fronts because it allows us to identify regions of contrasting air masses [19].

By analyzing geopotential height data, we can identify the location of fronts by looking for areas of sharp changes in height. Figure 4 plots the maps of GH for 500 mb level where the humidity demarcation was found to be maximum. GH maps also show the variations to be maximum at 01:00 UTC on May 12, 2022. Earlier studies by Jagdish et al. [2,3] have demonstrated a case where an atmospheric front detected is induced through ocean interactions.

Air-sea interactions over fronts are positively correlated to sea surface temperature (SST), indicating ocean forcing the atmosphere [20]. Studies emphasize that sensible heat fluxes associated with sea surface temperature (SST) fronts can impact evolution of atmospheric fronts [21]. Therefore, to gain further insight to the present case, the oceanic variables are further explored.

The actual SST and gradient fields on May 12, 2022 (Figure 5) show the presence of fronts as marked with the blue colored line. This front corresponds to the warmer eastern water mass and colder western water mass, respectively. The time evolution of SST and its gradient over the entire month of May as shown in Figure 6 shows that, between May 11, 2022, and about May 19, 2022, the SST front (observed by EOS-04 on May 12) was observed.

Here, it is important to note that on May 1–10, 2022, tropical cyclone Asani passed over the region, likely impacting the ocean atmosphere structure. The presence of cyclone Asani is shown in Figure 7, with the background ocean conditions represented by the average SST from May 1 to May 10, 2022. The overlaid box shows the future measurement area of the EOS-04 scanned on May 12. Prior to May 11, the ocean was warmer, which cooled off in the presence of cyclone Asani, similar to a recent study on the typhoon Lingling [22]. The time evolution of SST indicates that the ocean was warm before May 11, followed by a gradual cooling. After May 11, an SST front formed due to colder eastern waters and warmer western waters, which was observed by EOS-04. Similarly, the salinity over the box was less and consequently turned into high salinity as observed by May 12 implying cyclonic upwelling (figure not shown).

After the dissipation of a tropical cyclone, the oceanic and atmospheric conditions in the region may be significantly altered. One possible scenario is that the cyclone may have mixed the upper ocean,

Figure 4
Time series of geopotential height maps at 500 mb (07:00 UTC, May 11, 2022, to 11:00 UTC, May 12, 2022)

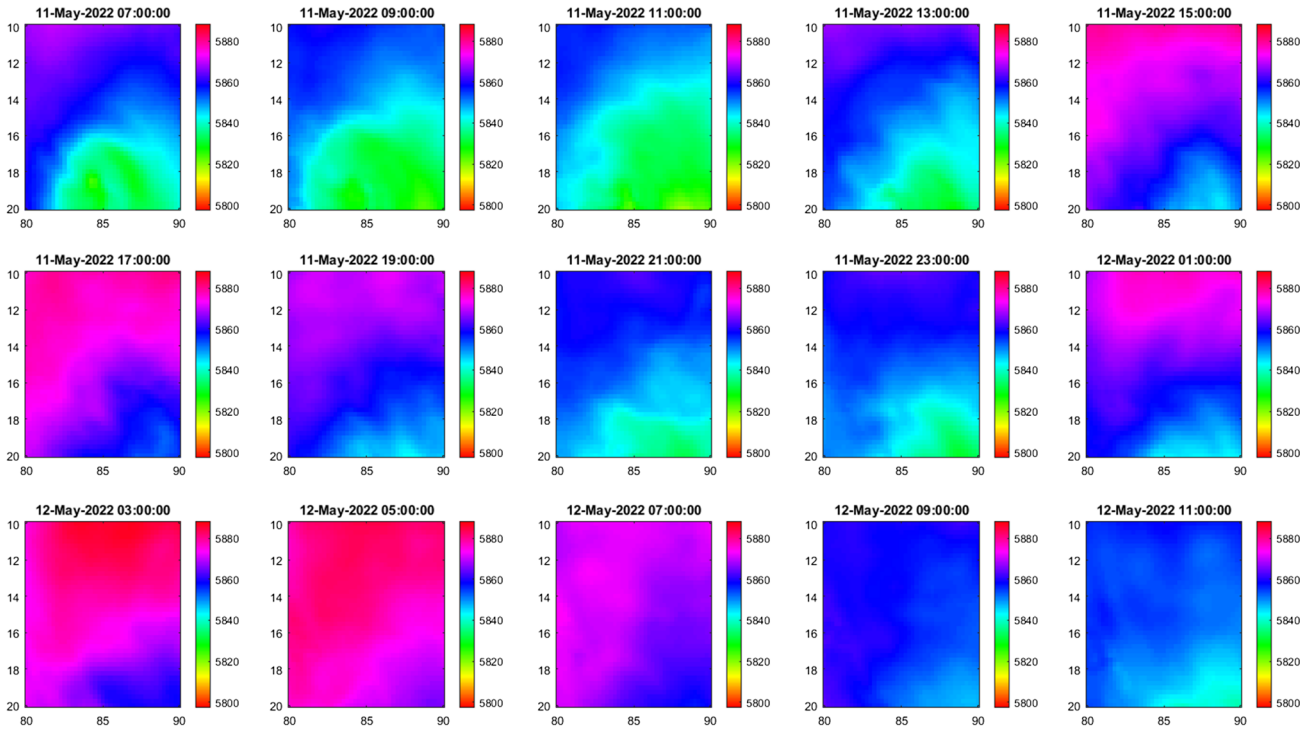

Figure 5
(a) GHRSST sea surface temperature and (b) its gradient over the scene location on May 12, 2022

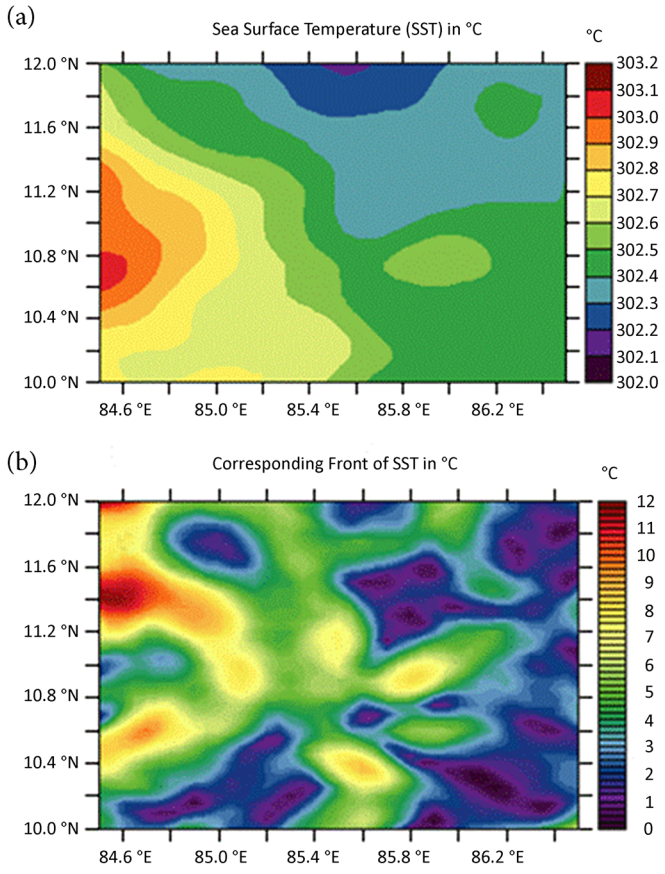

resulting in a shallower mixed layer and a more stable water column. This can create a horizontal gradient in the upper ocean properties, such as temperature, salinity, and nutrients, which can promote the formation of an oceanic front. In their paper, Yang et al. [22] highlighted the association of the low-level atmospheric cooling and frontogenesis after the passage of tropical cyclone.

At the same time, the dissipation of the cyclone can create a disturbance in the atmospheric circulation, resulting in the formation of an atmospheric front. As the cyclone dissipates, the associated low-pressure system weakens and moves away from the region, while the surrounding high-pressure systems move in to fill the void. This can create a horizontal gradient in atmospheric pressure, which can cause the formation of an atmospheric front.

Earlier studies [23–25] have also demonstrated the phenomenon of a tropical cyclone cold wake, which refers to a region of reduced SST that remains after the passage of a tropical cyclone and can persist for several weeks. This phenomenon results from two primary oceanic processes: strong cyclone winds induce turbulent mixing in the upper ocean layers, bringing colder subsurface water to the surface, and Ekman pumping, which transports deeper, colder water upward. The resulting cooling serves as a negative feedback mechanism, as the diminished ocean surface heat can inhibit further cyclone intensification. Studies indicate that cold wakes also exert broader and longer-term influences on the atmosphere and climate by suppressing rainfall, modifying atmospheric circulation, and altering air-sea heat fluxes within the affected region.

It is to be noted here that this cooling can also lead to a negative feedback that suppresses the storm's strength through a process called pressure adjustment [26]. The cooler water reduces the air-sea heat flux, leading to greater atmospheric stability and less air motion. This increased stability leads to changes in the storm's pressure field.

Recent studies [27, 28] have also reported thermodynamic processes that suppress cloud formation and precipitation over the cold wake area following the passage of the TC. After a tropical cyclone

Figure 6
(a) SST and (b) its gradient over the scene location for the entire month of May 2022

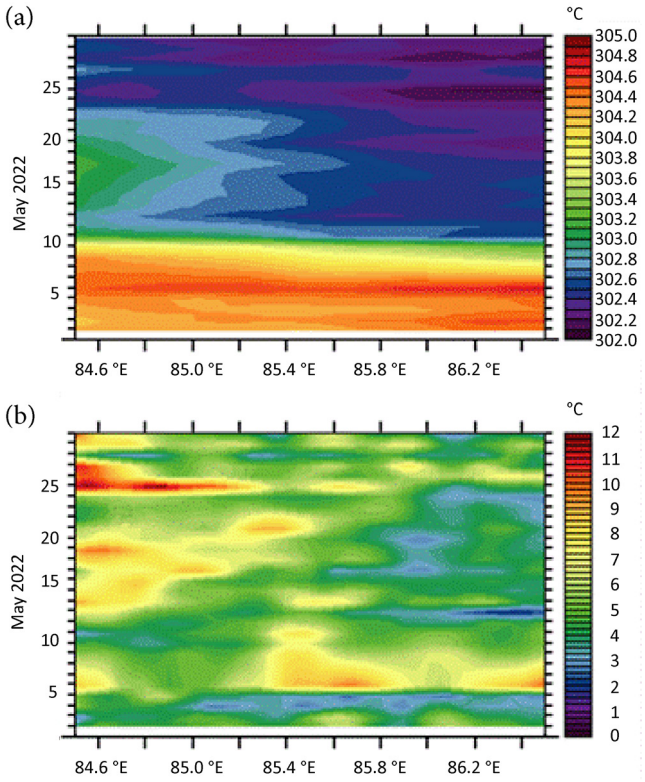

(TC) passes over warm ocean waters, it leaves a cold wake along its path. In this region, both surface sensible and latent heat fluxes are reduced. The decrease in sensible heat flux increases the stability of the boundary layer and inhibits upward air movement, as reflected by the relative divergence of surface winds perpendicular to the TC track. At the same time, reduced latent heat flux limits moisture supply at the air-sea interface.

The depletion of moisture and suppression of updrafts create favorable conditions for frontogenesis also in the atmospheric boundary layer, thus linking a sequential chain of events: passage of the cyclone, cold wake, thermodynamic forcing, and frontal evolution.

These chains of events can have a direct/indirect effect on the strength of the tropical cyclone. In the current case, it was reported by an earlier study [29] that the gravity wave potential energy for cyclone Asani was diminished, likely due to weaker convection and different environmental conditions.

It is also to be noted here that the oceanic and atmospheric fronts may interact with each other, affecting the exchange of heat, moisture, and momentum between the ocean and atmosphere. However, the presence of one does not guarantee the co-occurrence of the other in typical circumstances. However, in the present scenario, possibly due to the passage of a cyclone, both the ocean and atmosphere exhibit the signature of a front. This may be due to the latent heat released aloft after the passage of a cyclone, which can cause air masses to differ from one another in terms of temperature and density [30]. Simultaneously, the cyclone may also cause upwelling in the ocean, which generates the oceanic front [31]. Hence, post-cyclone conditions can lead to the coexistence of both oceanic and atmospheric front. The oceanic front may affect the location and intensity of the atmospheric front by influencing the atmospheric boundary layer, which in turn can affect the oceanic front by altering the surface fluxes. This interaction can lead to the development of complex feedback mechanisms that can influence the regional climate and ocean circulation patterns.

Figure 7
Cyclone Asani track (black line) overlaid on the background ocean conditions, between May 1 and 10, 2022

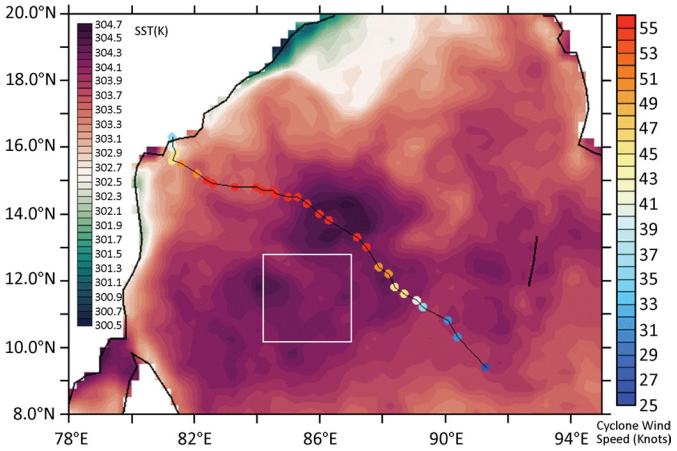

The exact mechanisms that lead to the formation of oceanic and atmospheric fronts after the dissipation of a tropical cyclone may vary depending on the specific conditions of the cyclone and the surrounding environment. However, understanding the dynamics of these fronts is important for predicting the post-cyclone conditions and for assessing the potential impacts on the oceanic and atmospheric systems.

5. Conclusion

In conclusion, this study documents a rare concurrent manifestation of oceanic and atmospheric frontal boundaries following the passage of a tropical cyclone, emphasizing the cold wake as a hotspot of dynamic air-sea coupling. The co-location of strong sea surface temperature gradients with atmospheric convergence and convective activity demonstrates the potential for feedbacks that extend cyclone influence well beyond its immediate passage. The present study unveils several key insights that contribute to our understanding of the intricate relationship between the atmosphere and the ocean. Through the analysis of observational data and modelling techniques, a linkage between atmospheric and oceanic fronts is unequivocally demonstrated. These results underscore the significance of the role of dry air intrusion in the formation and behavior of frontal boundaries. Furthermore, an interesting hypothesis emerges from this investigation, suggesting that the significant air-sea interaction observed can be attributed to the antecedent pathway of tropical cyclone Asani over the region. This notion posits that passage of a cyclone may induce frontogenesis in the MABL, thereby serving as a catalyst for the synergistic atmospheric and oceanic response witnessed. While it is not a requisite that every cyclone will inevitably generate a front, it has come to our attention that such an occurrence was observed in this specific case, as presented in the manuscript. This paper draws attention to the simultaneous manifestation of these three phenomena through the analysis of both model simulations and satellite data. These findings reinforce the importance of treating cold wake fronts not merely as passive oceanic features but as active modulators of atmosphere-ocean exchanges that shape regional weather, upper ocean biogeochemistry, and recovery timescales. However, it is important to acknowledge that, providing definitive, concrete proof may remain elusive. Nevertheless, we anticipate encountering similar instances with the aid of advanced sensor technology in the future. In addition, simulation studies with diverse conditions will clarify the interdependence and feedback loops further. Future research should prioritize integrated observing strategies that combine satellite, airborne, and in situ measurements with high-resolution coupled modeling to resolve the rapid evolution of

post-cyclone frontal systems. Particular focus on the roles of mesoscale and submesoscale processes, boundary layer adjustments, and biophysical feedbacks will be essential. Advancing this understanding will improve predictive capability of cyclone aftermath impacts, contribute to more skillful weather and climate forecasts, and refine our knowledge of ocean ecosystem responses to extreme atmospheric forcing.

Acknowledgement

The authors are grateful to the Director of the Space Applications Centre, Ahmedabad, and the Deputy Director of EPSA for their support and constant motivation.

Ethical Statement

This study does not contain any studies with human or animal subjects performed by any of the authors.

Conflicts of Interest

The authors declare that they have no conflicts of interest to this work.

Data Availability Statement

The data that support the findings of this study are openly available and are defined in the text.

Author Contribution Statement

Bipasha Paul Shukla: Conceptualization, Methodology, Software, Validation, Formal analysis, Investigation, Resources, Writing – original draft, Writing – review & editing, Visualization, Supervision, Project administration. **Suchandra Aich Bhowmick:** Formal analysis, Data curation, Writing – original draft, Writing – review & editing, Visualization. **Anup Kumar Mandal:** Software, Formal analysis, Data curation. **Abhisek Chakraborty:** Formal analysis, Data curation.

References

[1] Wei, X., Chong, J., Zhao, Y., Zhao, W., & Xu, Y. (2025). Atmospheric fronts detection and cold/warm type determination based on wind field retrieval from SAR imagery. *International Journal of Remote Sensing*, *46*(4), 1491–1516. https://doi.org/10.1080/01431161.2024.2431180

[2] Jagdish, Shukla, B. P., Chakraborty, A., Kumar, P., & Kumar, R. (2018). Atmospheric fronts using RISAT-1 SAR data: Case studies for shear lines. *IEEE Journal of Selected Topics in Applied Earth Observations and Remote Sensing*, *11*(12), 4711–4717. https://doi.org/10.1109/JSTARS.2018.2878753

[3] Jagdish, Shukla, B. P., Chakraborty, A., & Kumar, R. (2019). An interesting case of persistent rain cells observed by RISAT-1 SAR over the Indian Ocean during a pair of depression–cyclone interactions. *Remote Sensing Letters*, *10*(6), 545–552. https://doi.org/10.1080/2150704X.2019.1579377

[4] Jones, E., Parfitt, R., & Wing, A. A. (2024). Development of frontal boundaries during the extratropical transition of tropical cyclones. *Quarterly Journal of the Royal Meteorological Society*, *150*(759), 995–1011. https://doi.org/10.1002/qj.4633

[5] Zhang, H. (2023). Modulation of upper ocean vertical temperature structure and heat content by a fast-moving tropical cyclone. *Journal of Physical Oceanography*, *53*(2), 493–508. https://doi.org/10.1175/JPO-D-22-0132.1

[6] Parfitt, R., Czaja, A., Minobe, S., & Kuwano-Yoshida, A. (2016). The atmospheric frontal response to SST perturbations in the Gulf Stream region. *Geophysical Research Letters*, *43*(5), 2299–2306. https://doi.org/10.1002/2016GL067723

[7] Wu, X., He, Q., Shen, J., Peng, Z., Guo, L., Xie, W., & Lin, J. (2024). Different effects between cold front and tropical cyclone on short-term morphodynamics in the Changjiang Delta. *Journal of Marine Systems*, *243*, 103961. https://doi.org/10.1016/j.jmarsys.2023.103961

[8] Chakraborty, A., Sharma, N., Jaiswal, N., & Shukla, B. P. (2024). Probing atmospheric phenomena using C-band synthetic aperture radar onboard Earth Observation Satellite-04. *Current Science*, *126*(9), 1118–1125. https://doi.org/10.18520/cs/v126/i9/1118-1125

[9] Asif, Z., Chen, Z., An, C., & Dong, J. (2022). Environmental impact and challenges associated with oil spill on shorelines. *Journal of Marine Science and Engineering*, *10*(6), 762. https://doi.org/10.3390/jmse10060762

[10] Wang, C., Mouche, A., Tandeo, P., Stopa, J. E., Longépé, N., Erhard, G., & Chapron, B. (2019). A labelled ocean SAR imagery dataset of ten geophysical phenomena from Sentinel-1 wave mode. *Geoscience Data Journal*, *6*(2), 105–115. https://doi.org/10.1002/gdj3.73

[11] Subrahmanyam, K. V., Bothale, R. V., Swapna, M., & Chauhan, P. (2023). Deciphering the signatures of oceanic convective rain cells using simultaneous observations from C-band synthetic aperture radar onboard EOS-04 satellite and GPM measurements. *Geophysical Research Letters*, *50*(5), e2022GL102317. https://doi.org/10.1029/2022GL102317

[12] Hersbach, H., Bell, B., Berrisford, P., Hirahara, S., Horányi, A., Muñoz-Sabater, J., & Thépaut, J. N. (2020). The ERA5 global reanalysis. *Quarterly Journal of the Royal Meteorological Society*, *146*, 1999–2049. https://doi.org/10.1002/qj.3803

[13] Reynolds, R. W., Smith, T. M., Liu, C., Chelton, D. B., Casey, K. S., & Schlax, M. G. (2007). Daily high-resolution-blended analyses for sea surface temperature. *Journal of Climate*, *20*(22), 5473–5496. https://doi.org/10.1175/2007JCLI1824.1

[14] Chin, T. M., Cuervo, J. V., & Armstrong, E. M. (2017). A multi-scale high-resolution analysis of sea surface temperature. *Remote Sensing of Environment*, *200*, 154–169. https://doi.org/10.1016/j.rse.2017.07.029

[15] Sharma, S., Tripathi, S., Sowkhya, B., Arora, P., Tyagi, S., Sanid, C., Agarawal, R., & Babu, K. N. (2024). Assessment of EOS-04 (RISAT-1A) data calibration. *Current Science*, *126*, 1033–1040. https://doi.org/10.1175/2007JCLI1824.110.18520/cs/v126/i9/1033-1040

[16] Ullman, D. S., & Cornillon, P. C. (2000). Evaluation of front detection methods for satellite-derived SST data using in situ observations. *Journal of Atmospheric and Oceanic Technology*, *17*(12), 1667–1675. https://doi.org/10.1175/1520-0426(2000)017%3C1667:EOFDMF%3E2.0.CO;2

[17] Qu, L., Thomas, L. N., Wienkers, A. F., Hetland, R. D., Kobashi, D., Taylor, J. R., … & Nash, J. D. (2022). Rapid vertical exchange at fronts in the Northern Gulf of Mexico. *Nature Communications*, *13*(1), 5624. https://doi.org/10.1038/s41467-022-33251-7

[18] Rizzi, R., Rotunno, R., & Bryan, G. (2021). A thermodynamic perspective on steady-state tropical cyclones. *Journal of the Atmospheric Sciences*, *78*(2), 583–593. https://doi.org/10.1175/JAS-D-20-0140.1

[19] Volonté, A., Turner, A. G., Schiemann, R., Vidale, P. L., & Klingaman, N. P. (2022). Characterising the interaction of tropical and extratropical air masses controlling East Asian summer monsoon progression using a novel frontal detection

approach. *Weather and Climate Dynamics*, *3*(2), 575–599. https://doi.org/10.5194/wcd-3-575-2022

[20] Frankignoul, C., Hall, R., Kwon, Y., & Czaja, A. (2025). On the atmospheric response to Oyashio extension front disturbance and mesoscale SST variations. *Journal of Climate*, *38*(18), 5055–5066. https://doi.org/10.1175/JCLI-D-25-0083.1

[21] Reeder, M. J., Spengler, T., & Spensberger, C. (2021). The effect of sea surface temperature fronts on atmospheric frontogenesis. *Journal of Atmospheric Sciences*, *78*(1), 1753–1771. https://doi.org/10.1175/JAS-D-20-0118.1

[22] Yang, S., Moon, I. J., Bae, H. J., Kim, B. M., Byun, D. S., & Lee, H. Y. (2022). Intense atmospheric frontogenesis by air–sea coupling processes during the passage of Typhoon Lingling captured at Ieodo Ocean Research Station. *Scientific Reports*, *12*(1), 15513. https://doi.org/10.1038/s41598-022-19359-2

[23] Akhila, R. S., Kuttippurath, J., Balan Sarojini, B., Chakraborty, A., & Rahul, R. (2022). Observed tropical cyclone-driven cold wakes in the context of rapid warming of the Arabian Sea. *Journal of Operational Oceanography*, *16*(3), 236–251. https://doi.org/10.1080/1755876X.2022.2068260

[24] Bhowmick, S., Agarwal, N., Sharma, R., Sundar, R., Venkatesan, R., Prasad, A., & Navaneeth, K. N. (2020). Cyclone Amphan: Oceanic conditions pre-and post-cyclone using in situ and satellite observation. *Current Science*, *119*(9), 1510–1516.

[25] Ling, Z., Chen, Z., Wang, G., He, H., & Chen, C. (2021). Recovery of tropical cyclone induce SST cooling observed by satellite in Northwestern Pacific Ocean. *Remote Sensing*, *13*(18), 3781. https://doi.org/10.3390/rs13183781

[26] Lindzen, R. S., & Nigam, S. (1987). On the role of sea surface temperature gradients in forcing low-level winds and convergence in the tropics. *Journal of Atmospheric Sciences*, *44*(17), 2418–2436. https://doi.org/10.1175/1520-0469(1987)044%3C2418:OTROSS%3E2.0.CO;2

[27] Ma, Z., Fei, J., Lin, Y., & Huang, X. (2020). Modulation of clouds and rainfall by tropical cyclone's cold wakes. *Geophysical Research Letters*, *47*(17), e2020GL088873. https://doi.org/10.1029/2020GL088873

[28] Pasquero, C., Desbiolles, F., & Meroni, A. N. (2021). Air-sea interactions in the cold wakes of tropical cyclones. *Geophysical Research Letters*, *48*(2), e2020GL091185. https://doi.org/10.1029/2020GL091185

[29] Nanda, K., Sasmal, S., Hazra, R., Datta, A., Panchadhyayee, P., & Potirakis, S. M. (2025). Study on the distribution of Gravity Wave (GW) activity in six Bay of Bengal tropical cyclones. *Atmosphere*, *16*(2), 235. https://doi.org/10.3390/atmos16020235

[30] Igel, A., & Heever, S. (2014). The role of latent heating in warm frontogenesis. *Quarterly Journal of the Royal Meteorological Society*, *140*(678), 139–150. https://doi.org/10.1002/qj.2118

[31] Singh, V. K., & Roxy, M. K. (2022). A review of ocean-atmosphere interactions during tropical cyclones in the north Indian Ocean. *Earth-Science Reviews*, *226*, 103967. https://doi.org/10.1016/j.earscirev.2022.103967

How to Cite: Shukla, B. P., Bhowmick, S. A., Mandal, A. K., & Chakraborty, A. (2026). Observing the Linkage of Atmospheric and Oceanic Front Using Remote Sensing Observations: A Case Study After the Passage of Tropical Cyclone Asani. *Remote Sensing for Sustainable Oceans*. https://doi.org/10.47852/bonviewRSSO62026936